ECS Transactions, 35 (4) 909-921 (2011)
10.1149/1.3572328 ©The Electrochemical Society

# Reliability Properties and Current Conduction Mechanisms of $HfO_2$ MIS Capacitor with Dual Plasma Treatment

Kow-Ming Chang[a,b], Ting-Chia Chang[a,*], Shou-Hsien Chen[a], and I-Chung Deng[c]

[a] Department of Electronics Engineering & Institute of Electronics, National Chiao Tung University, 1001 Ta Hsueh Road, Hsinchu, Taiwan 30010, R.O.C.
[b] College of Electrical and Information Engineering, I-Shou University, Kaohsiung, Taiwan 84001, R.O.C.
[c] Department of Electronic Engineering, Technology and Science Institute of Northern Taiwan

The incorporation of nitrogen in $HfO_2$ gate dielectrics has been reported to be beneficial for electrical performance. The improvement in the electrical characteristics of $HfO_2$ thin film with plasma nitridation process or plasma fluorination process has also been examined. In this study, dual plasma, $CF_4$ pre-treatment and nitrogen post-treatment, treatments were performed on $HfO_2$ MIS capacitor for further improvement on reliability characteristic. We examine the reliability properties and the current conduction mechanism of $HfO_2$ thin films. The frequency dispersion and constant voltage stress (CVS) characteristics of the samples were analyzed to estimate the improvement. According to the present study, dual plasma treatment could be better than single plasma treatment and would be an effective approach for $HfO_2$ dielectric improvement.

## Introduction

The rapid progress of complementary metal oxide semiconductor (CMOS) integrated circuit technology has met several serious technological challenges over the past few years. According to the prediction of the International Technology Roadmap for Semiconductor (ITRS), the conventional gate dielectric layer will reach its physical limits [1]. Gate dielectric scaling of CMOS will increase the speed and the packing density of modern circuits. However, the aggressive shrinking of the gate length and gate dielectric thickness accompanies excessive leakage current and reliability problems. To solve these problems, a major solution is to replace the traditional $SiO_2$ or SiON by other higher dielectric constant material. Using high dielectric constant material for gate dielectric could have larger physical thickness and maintain smaller equivalent oxide thickness (EOT). As a result, high-dielectric-constant (high-κ) thin films have been considered as suitable gate dielectric for modern CMOS technology. There are various high-κ thin film has been investigated [2-4]. Among these high-κ materials, $HfO_2$ is considered as the most promising candidate because of high dielectric constant (~25), wide band gap (~5.7 eV), and large band offset with Si conduction band (~1.5 eV) [2, 5]. Nevertheless, there are still some issues which need to be considered, such as the reliability and thermal stability of the dielectrics [6, 7].

It has been reported that nitrogen incorporated into $HfO_2$ gate dielectrics has beneficial effect on performance [8]. Nitrogen could be incorporated into dielectric layer by ICP plasma nitridation process at lower temperature [9, 10]. As reported in previous study: nitrogen incorporation can suppress crystallization during high temperature treatment, reduce dopant penetration, increase dielectric constant, and reduce leakage current by about 3-4 orders of magnitude [11, 12]. Umezawa et al [13] noted that nitrogen could deactivate the oxygen vacancy related states within $HfO_2$ band gap. The absence of gap states leads to the removal of electron leakage path.

In addition, the incorporation of fluorine in $HfO_2$ gate dielectrics also has been reported to be beneficial for electrical and reliability performance [14-16]. The quality of interfacial layer (IL) becomes more and more important due to gate dielectric scaling. Wong et al [17] noted that the applied electric field would be largely distributed in the low-κ region for high-κ/low-κ stack layer because of Gauss's law. The first breakdown happened in the low-κ layer [17]. Recently, several studies have used fluorine incorporation to improve IL quality at $HfO_2$/Si interface because Si-F bond (5.73 eV) is stronger than Si-H bond (3.18eV) [18, 19]. Moreover, pre-$CF_4$ plasma treatment has been shown to effectively suppress the IL formation [20].

In this study, we propose to combine two kinds of plasma treatment (denoted as dual plasma treatment), $CF_4$ pre-treatment and nitrogen post-treatment, in order to achieve further improvement. We have examined the reliability properties and the current conduction mechanism of $HfO_2$ MIS capacitor structure. First of all, the capacitance-voltage (C-V) characteristics and current-voltage (J-V) characteristics will be briefly described. Second, the frequency dispersion and constant voltage stress (CVS) characteristics of the samples will be analyzed to estimate the improvement. Finally, current conduction mechanisms, such as Schottky emission, Frenkel-Poole (F-P) emission, and Fowler-Nordheim (F-N) tunneling will be discussed. Schottky barrier height, F-P barrier height, and F-N barrier height will be extracted.

## Experimental

After standard RCA cleaning, the samples were treated in $CF_4$ plasma (denoted as $CF_4$ pre-treatment) for various times. The substrate temperature in a plasma enhanced chemical vapor deposition (PECVD) system was set at 300 $^oC$. The process pressure and the $CF_4$ flow rate were 500 mTorr and 100 sccm, respectively. The RF power was set at 20 W and the exposure times were varied in the range of 10-40 sec. After $CF_4$ pre-treatment, $HfO_2$ thin film was deposited on the samples by the metal organic chemical vapor deposition (MOCVD) system. Then post deposition annealing (PDA) was performed at 600 $^oC$ for 30 sec in a rapid temperature annealing (RTA) system. After PDA, samples were nitrided in nitrogen plasma (denoted as nitrogen post-treatment) by PECVD. The flow rate of nitrogen gas, which is $N_2$ or $NH_3$, was set at 100 sccm. Post nitridation annealing (PNA) was performed with RTA equipment at 600 $^oC$ for 30 sec in order to reduce plasma damage. Thereafter, 40 nm-Ti films and 400 nm Al films were deposited by e-beam evaporation system. The top electrodes were defined lithographically and etched to define a gate area of 5000 $\mu m^2$. Finally, backside Al electrodes were deposited by the thermal evaporation to form the Ohmic contact. The capacitance-voltage (C-V) and current-voltage (I-V) characteristics of MIS structure were measured by using a C-V measurement (Hewlett-Packard 4284) and Hewlett-Packard

4156C semiconductor parameter analyzer, respectively. The condition of frequency dispersion measurement was set as from 1 kHz to 100 kHz. The stress condition of CVS measurement was set as a constant voltage -3V for 0 to 500 sec. Furthermore, the I-V characteristics were measured at elevated temperatures from 25 to 125 $^{o}$C, 25 $^{o}$C per step, in order to analyze current conduction mechanisms.

## Results and Discussion

C-V and J-V Characteristics

Figure 1 shows the C-V characteristics of the $HfO_2$ thin films treated in $CF_4$ plasma for different process durations and $N_2$ plasma for 120 sec. The frequency used in the high frequency C-V measurement was set at 50 kHz. The sample was treated only in $N_2$ plasma for 120 sec (RF power = 50 W) shows much higher capacitance density than the sample with no treatment. The higher capacitance could be attributed to the PDA process [21-23] and the nitrogen incorporation in the $HfO_2$ thin film. The nitrogen incorporation could enhance the electronic polarization as well as the ionic polarization, which result in the increase of dielectric constant [12, 24]. On the other hand, the capacitance density and interface characteristics show further improvement with the combination of $CF_4$ pre-treatment for 10 sec and $N_2$ post-treatment for 120 sec. With $CF_4$ pre-treatment, fluorine atoms would pile up at the $HfO_2$/Si interface, improve the quality of interface [19], and suppress the IL formation [20]. Besides, for $CF_4$ pre-treatment times longer than 10 sec, the plasma damage caused the degradation of $HfO_2$/Si interface and the degradation of capacitance density.

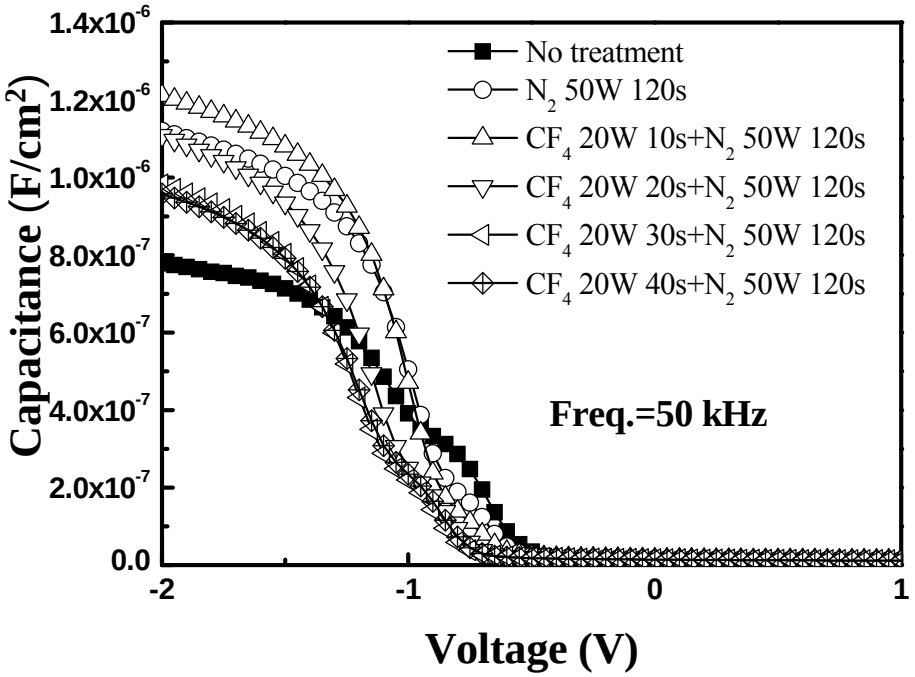


Figure 1. The C-V characteristics of the $HfO_2$ thin films treated in $CF_4$ plasma for different process durations and $N_2$ plasma for 120 sec.

Figure 2 shows the J-V characteristics of the $HfO_2$ thin films treated in $CF_4$ plasma for different process durations and $N_2$ plasma for 120 sec. Compared with the sample with no treatment, the gate leakage current decreased by about 4 orders of magnitude for the sample with $CF_4$ pre-treatment for 10 sec and $N_2$ post-treatment for 120 sec. The reduction of the gate leakage could be attributed to defect passivation. Oxygen vacancy related states and interface states could be passivated by nitrogen and fluorine atoms [13, 16]. On the other hand, for $CF_4$ pre-treatment times longer than 10 sec, the plasma damage caused the degradation of interface and the increase of gate leakage current. The best condition of dual plasma treatment is as follows: $CF_4$ pre-treatment (time=10s, RF Power=20W) and $N_2$ post-treatment (time=120s, RF Power=50W). The gate leakage of the sample with best condition is $1.05 \times 10^{-5}$ A/cm$^2$ at $V_g$ = -1.5 V.

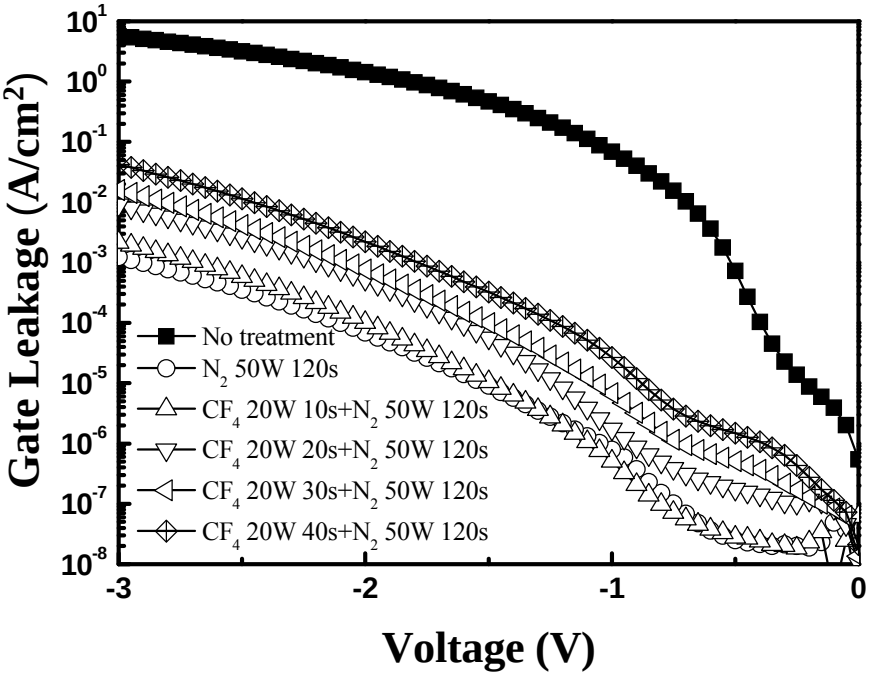


Figure 2. The J-V characteristics of the $HfO_2$ thin films treated in $CF_4$ plasma for different process durations and $N_2$ plasma for 120 sec.

In Figure 3 and Figure 4, the C-V and the J-V characteristics of the $HfO_2$ gate dielectrics, treated in $CF_4$ plasma for different process durations and $NH_3$ plasma for 120 sec, are presented. The RF power of $NH_3$ post-treatment was set at 40 W. As mentioned before, the reason of the improvement in the $NH_3$ plasma nitridation process could be the same as the one in the $N_2$ plasma nitridation process. From the similar analysis, the best condition of dual plasma treatment is as follows: $CF_4$ pre-treatment (time=10s, RF Power=20W) and $NH_3$ post-treatment (time=120s, RF Power=40W). The gate leakage of the sample with best condition is $1.62 \times 10^{-5}$ A/cm$^2$ at $V_g$ = -1.5 V. In summary, C-V and I-V Characteristics could be further improved by dual plasma treatment.

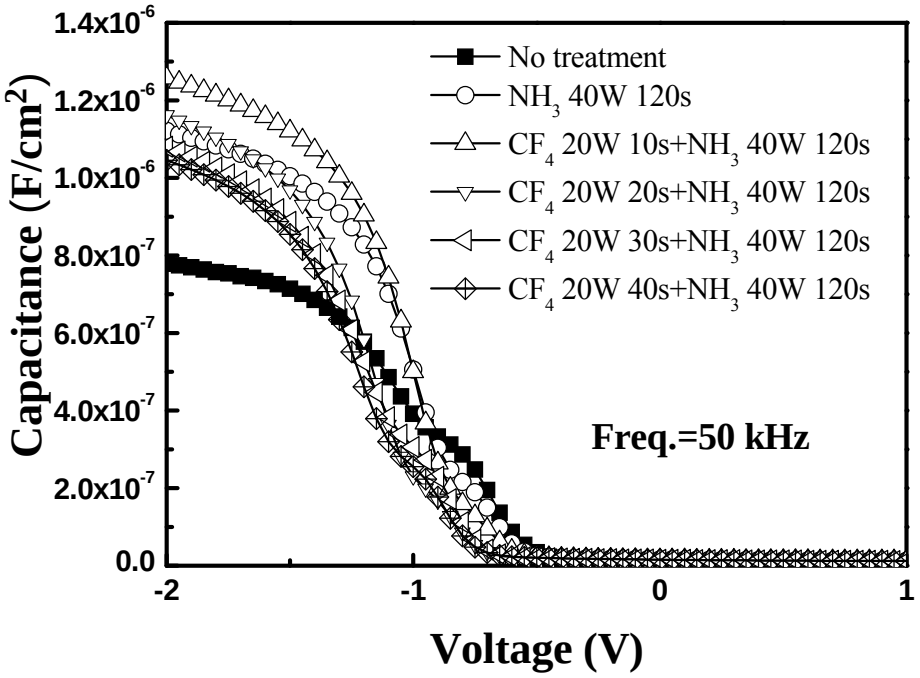


Figure 3. The C-V characteristics of the $HfO_2$ thin films treated in $CF_4$ plasma for different process durations and $NH_3$ plasma for 120 sec.

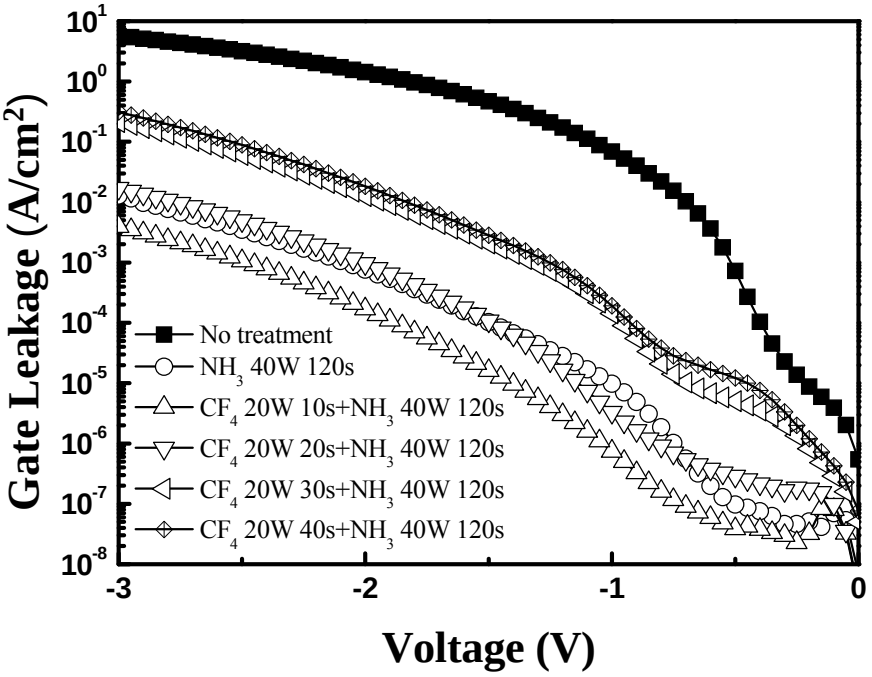


Figure 4. The J-V characteristics of the $HfO_2$ thin films treated in $CF_4$ plasma for different process durations and $NH_3$ plasma for 120 sec.

Frequency Dispersion Characteristics

The C-V characteristics of the $HfO_2$ thin films, treated with $CF_4$ plasma for different process durations and $N_2$ plasma for 120 sec, have been measured as a function of frequency as shown in Figure 5. The measurements were made in the frequency range of 1-100 kHz (1, 10, and 100 kHz). Frequency dispersion could be observed because of the response of trap charges to signal frequency. At low frequencies, interface traps generated the additional capacitance because some of traps could follow the change of gate voltage [25]. The frequency dispersion in the accumulation region and the hump in the depletion region are significant for the sample with no treatment. The sample treated by $N_2$ plasma showed relatively smaller frequency dispersion and smaller hump than the sample with no treatment. On the other hand, it was obvious that the sample treated by $CF_4$ pre-treatment for 10 sec and $N_2$ post-treatment for 120 sec exhibited nearly no dispersion in the accumulation region and nearly no hump in the depletion because interface states could be improved effectively [25-28] by dual plasma treatment. However, the frequency dispersion and the hump became severe again when the $CF_4$ pre-treatment time is longer than 10 sec owing to plasma damage at interface.

Figure 6 displays the C-V frequency dependence of the $HfO_2$ thin films treated in $CF_4$ plasma for different process durations and $NH_3$ plasma for 120 sec. The sample treated by $CF_4$ pre-treatment for 10 sec and $NH_3$ post-treatment for 120 sec exhibited nearly no dispersion and nearly no hump during C-V measurement. This indicated that dual plasma treatment could effectively eliminate interface states and greatly enhance IL quality than single plasma treatment.

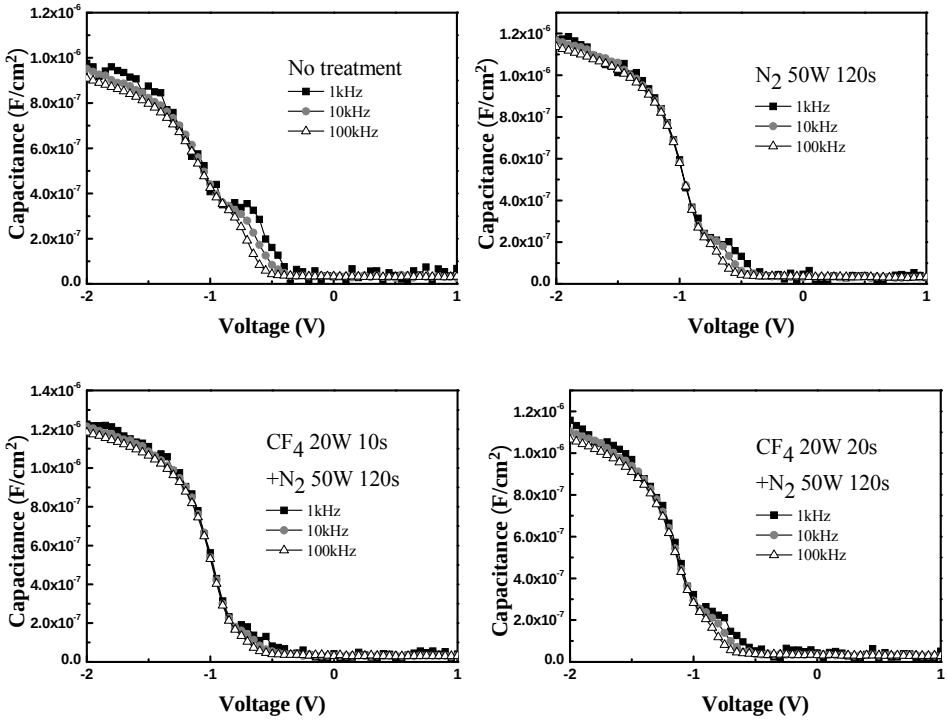


Figure 5. C-V frequency dependence of the $HfO_2$ thin films treated in $CF_4$ plasma for different process durations and $N_2$ plasma for 120 sec.

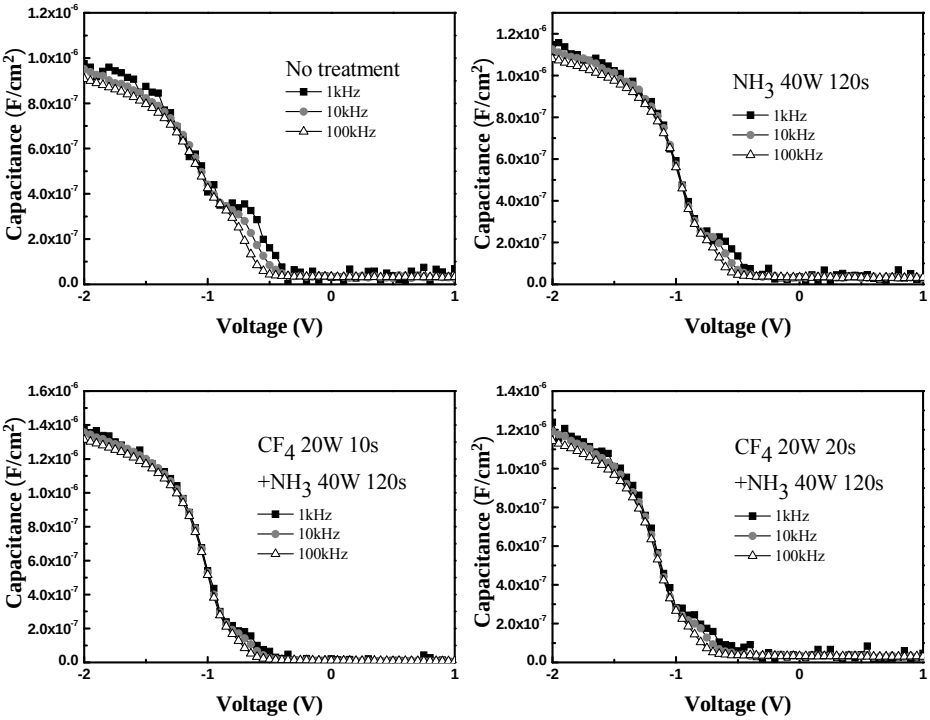


Figure 6. C-V frequency dependence of the $HfO_2$ thin films treated in $CF_4$ plasma for different process durations and $NH_3$ plasma for 120 sec.

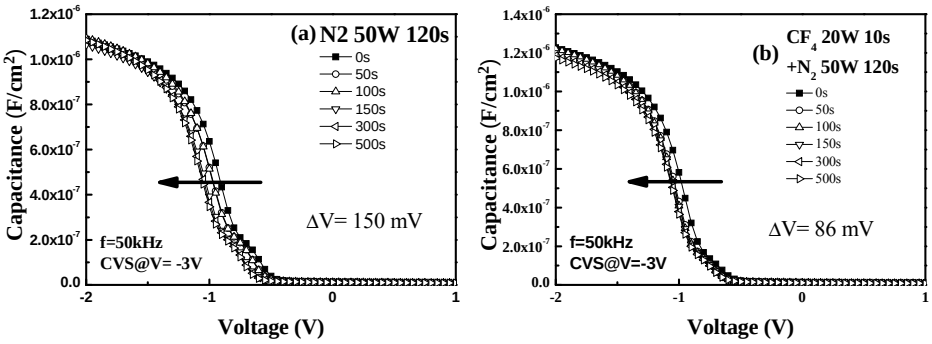


Figure 7. The C-V curves before and after CVS characteristics of the $HfO_2$ thin films treated by (a) single plasma treatment and (b) dual plasma treatment.

Constant Voltage Stress Characteristics

Figure 7 displays the C-V curves before and after CVS testing of the $HfO_2$ thin films treated by $N_2$ plasma post-treatment (as shown in Figure 7(a)) and the combination of $CF_4$ plasma pre-treatment and $N_2$ plasma post-treatment (as shown in Figure 7(b)), respectively. The stress voltage was set at -3 V. The stress times were made in a range from 0 to 500 sec. All the C-V curves shift to left as stress time increase indicated that there were positive charges trapped in the high-κ dielectric layer. Trapping of positive charges could be explained by Anode hole injection model [29]. During constant negative bias stress at a fixed gate voltage, the injected electrons traveled through dielectric and

arrived at the interface. These electrons gained energy to liberate the hydrogen at the interface, leading to the generation of Si dangling bond. The liberated hydrogen diffused into the dielectric through the oxide field, trapped in the dielectric, leading to the creation of positively charged centers [30, 31]. The C-V curves had smaller $V_{fb}$ shift and less distortion for samples with dual plasma treatment, indicating that samples with dual plasma treatment had less interface trap charges generated at the dielectric/Si interface and had better reliability properties than samples with single plasma treatment.

Schottky Emission

Figure 8(a) depicts the J-E plots for the sample with no treatment at different temperatures from 298 K to 398 K (25 K per step). The inset of Figure 8(a) is the band diagram demonstrating Schottky emission. The electric field E is an "effective" electric field (E = V/CET), while capacitance effective thickness (CET) is extracted from the capacitance density in the accumulation region [32]. The standard Schottky emission could be expressed as

$$J_{SE} = A^* T^2 \exp\left[\frac{-q\left(\phi_B - \sqrt{qE/4\pi\varepsilon_r\varepsilon_0}\right)}{kT}\right], \qquad A^* = 120\frac{m^*}{m_0}\left(\frac{A}{cm^2K^2}\right), \tag{1}$$

where $J_{SE}$ is the current density, $A^*$ is the effective Richardson constant, E is the effective electric field, T is the absolute temperature, q is the electron charge, $q\phi_B$ is the Schottky barrier height, k is Boltzmann's constant, $\varepsilon_0$ is the permittivity of free space, $\varepsilon_r$ is the dynamic dielectric constant, $m^*$ is the electron effective mass in $HfO_2$, $m_0$ is the free electron mass. The electron effective mass is 0.1 $m_0$ [33, 34].

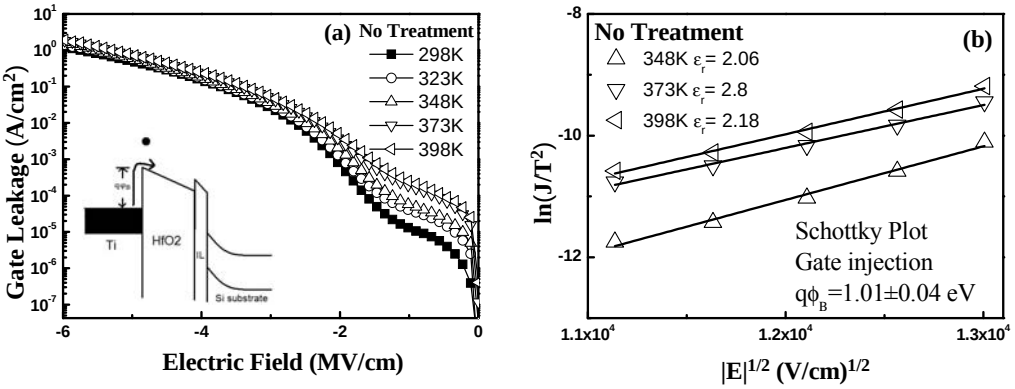


Figure 8. (a) The J-E curves at various temperatures and (b) Schottky emission plots, $\ln(J/T^2)$ versus $E^{1/2}$, for the $HfO_2$ thin film with no treatment.

For the standard Schottky emission, a plot of $\ln(J/T^2)$ versus $E^{1/2}$ should be a straight line, as shown in Figure 8(b). It was found that Schottky emission is the dominate conduction mechanism in the region of low to medium electric fields (1.7 - 3.0 MV/cm) [35]. Eq. (2) expresses the intercept of the Schottky emission plot with the vertical axis. The barrier height can be extracted from Eq. (2).

$$Intercept = \ln(A^*) - \frac{q\phi_B}{kT}, \quad A^* = 120\frac{m^*}{m_0}\ (\frac{A}{cm^2K^2}). \tag{2}$$

Because of effective electric field (E = V/CET), the extracted barrier heights in this study are effective barrier heights. The extracted Schottky barrier heights for the samples with no treatment, single plasma treatment, and dual plasma treatment are listed in Table I. It is clear that the samples had larger barrier height than other samples after $CF_4$ pre-treatment for 10 sec and nitrogen post-treatment for 120 sec.

**TABLE I.** Schottky Barrier Height Extracted for The Samples with No Treatment, Single Plasma Treatment, and Dual Plasma Treatment.

| **Barrier height** | **No treatment** | **$N_2$, 120s** | **$CF_4$, 10s + $N_2$, 120s** | **$CF_4$, 20s + $N_2$, 120s** |
|---|---|---|---|---|
| $q\phi_B(eV)$ | 1.01±0.04 | 1.23±0.09 | 1.32±0.1 | 1.19±0.09 |
| **Barrier height** | **No treatment** | **$NH_3$, 120s** | **$CF_4$, 10s + $NH_3$, 120s** | **$CF_4$, 10s + $NH_3$, 120s** |
| $q\phi_B(eV)$ | 1.01±0.04 | 1.21±0.04 | 1.32±0.07 | 1.21±0.07 |

Frenkel-Poole (F-P) Emission

When gate under negative bias, electrons will inject from gate into $HfO_2$ dielectric layer and will be trapped into shallow trap levels. Thereafter, the electrons transported through the dielectric layer by hopping between these trap levels, leading to leakage current, called Frenkel-Poole (F-P) emission. The standard F-P emission could be expressed as [35]

$$J_{FP} = C_t E \exp\left[\frac{-q(\phi_t - \sqrt{qE/\pi\varepsilon_r\varepsilon_0})}{kT}\right], \tag{3}$$

where $J_{FP}$ is the current density, E is effective electric field, $C_t$ is a constant proportional to the density of bulk oxide traps, $q\phi_t$ is the trap energy in $HfO_2$, and other parameters are as defined earlier. For the standard Frenkel-Poole emission, a plot of $\ln(J_{FP}/E)$ versus $E^{1/2}$ should be linear. It was found that F-P emission is the dominate conduction mechanism in the region of medium to high electric fields (4.0 - 6.0 MV/cm). The trap energy in dielectric layer could be extracted form good F-P fitting, as shown in Figure 9.

Table II lists the trap energy levels of the samples with no treatment, single plasma treatment, and dual plasma treatment. The extracted trap levels for the sample with and without $N_2$ post-treatment were 1.12 eV and 0.72 eV, respectively. In contrast, the trap level for the sample treated by $CF_4$ pre-treatment for 10 sec and $N_2$ post-treatment for 120 sec was 1.14 eV. The deeper trap level means that most of shallow trap levels in $HfO_2$ thin film can be eliminated [32] by using dual plasma treatment. The elimination of shallow trap levels resulted in the reduction of F-P conduction current. Similarly, the sample treated in $CF_4$ pre-treatment for 10 sec and $NH_3$ post-treatment for 120 sec also exhibited larger trap levels than other samples. In short, dual plasma

treatment could eliminate the shallow trap levels and greatly reduce the gate leakage current.

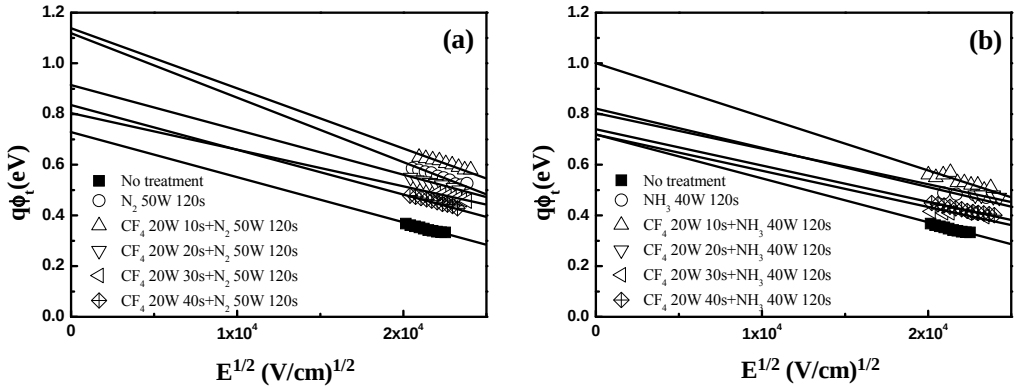


Figure 9. Trapping energy levels extracted from F-P fitting for the samples with dual plasma treatment (a) $CF_4$ plasma and $N_2$ plasma (b) $CF_4$ plasma and $NH_3$ plasma.

**TABLE II.** F-P Trapping Level Extracted for The Samples with No Treatment, Single Plasma Treatment, and Dual Plasma Treatment.

| **Barrier height** | **No treatment** | **$N_2$, 120s** | **$CF_4$, 10s + $N_2$, 120s** | **$CF_4$, 20s + $N_2$, 120s** |
|---|---|---|---|---|
| $q\phi_t(eV)$ | 0.72 | 1.12 | 1.14 | 0.91 |
| **Barrier height** | **No treatment** | **$NH_3$, 120s** | **$CF_4$, 10s + $NH_3$, 120s** | **$CF_4$, 10s + $NH_3$, 120s** |
| $q\phi_t(eV)$ | 0.72 | 0.82 | 1.10 | 0.80 |

Fowler-Nordheim (F-N) Tunneling

In higher electric field, the Fowler-Nordheim (F-N) tunneling dominated the conduction mechanism [36]. The standard F-P emission could be expressed as

$$J_{FN} = AE^2 \exp\left[\frac{-8\pi\sqrt{2m^*}\left(q\phi_f\right)^{3/2}}{3qhE}\right], \quad (4)$$

where $J_{FN}$ is the current density, h is the Plunk's constant, $q\phi_f$ is the potential barrier height, $m^*$ is the electron effective mass in $HfO_2$, and the other notations were as same as mentioned before. The electron effective mass here is 0.1 $m_0$ [33, 34]. If the leakage current is dominated by the F-N mechanism, a plot of $\ln(J/E^2)$ versus 1/E should be linear. Linear characteristic could be observed at high electric field (> 7 MV/cm), as shown in Figure 10. The slope of each curve in Figure 10 and Eq. (5) could obtain the F-N barrier height, which were listed in Table III.

$$\phi_f = \left( \frac{9h^2}{128\pi^2 m^* q} \right) * (slope)^{2/3} . \quad (5)$$

Table III listed the F-N barrier height of the samples with no treatment, single plasma treatment, and dual plasma treatment. It could be observed that samples treated in $CF_4$ pre-treatment for 10 sec and nitrogen post-treatment for 120sec had larger value than other samples. The injection of electrons from the gate entered the conduction band of $HfO_2$ by tunneling through a triangular potential barrier. The injected electrons interacted with lattice or transferred its energy at anode [37], which resulted in the degradation of the dielectric layer. As a result, the sample with proper dual plasma treatment had bigger F-N barrier height and better reliability properties.

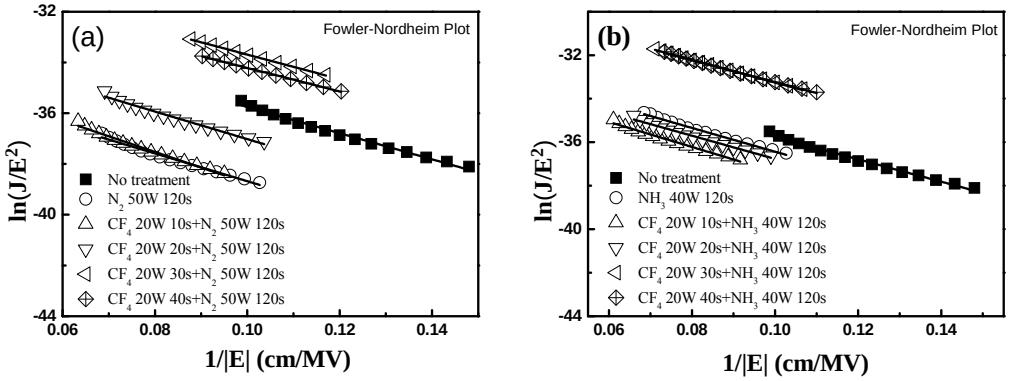


Figure 10. F-N tunneling characteristic, $\ln(J/E^2)$ vs. 1/E, for the samples with dual plasma treatment (a) $CF_4$ plasma and $N_2$ plasma (b) $CF_4$ plasma and $NH_3$ plasma

**TABLE III.** F-N Barrier Height Extracted for The Samples with No Treatment, Single Plasma Treatment, and Dual Plasma Treatment.

| **Barrier height** | **No treatment** | **$N_2$, 120s** | **$CF_4$, 10s + $N_2$, 120s** | **$CF_4$, 20s + $N_2$, 120s** |
|---|---|---|---|---|
| $q\phi_f(eV)$ | 1.78 | 1.86 | 2.01 | 1.85 |
| **Barrier height** | **No treatment** | **$NH_3$, 120s** | **$CF_4$, 10s + $NH_3$, 120s** | **$CF_4$, 10s + $NH_3$, 120s** |
| $q\phi_f(eV)$ | 1.78 | 1.86 | 1.92 | 1.83 |

## Conclusion

In conclusion, the reliability properties and current conduction mechanisms of $HfO_2$ gate dielectric films as a function of dual plasma treatment (the combination of $CF_4$ pre-treatment and nitrogen post-treatment) have been investigated. First, the best conditions which decided form C-V and J-V characteristics were the samples treated by $CF_4$ plasma for 10 sec and $N_2$ ($NH_3$) plasma for 120 sec. According to the current conduction analysis, the dominant current conduction mechanism was Schottky emission type in the region of low to medium electric fields (1.7 – 3.0 MV/cm); Frenkel-Poole (F-P) emission operated in the region of medium to high fields (4.0 – 6.0 MV/cm); Fowler-

Nordheim (F-N) tunneling was dominant at high fields (> 7 MV/cm). Dual plasma treatment was effective in improving interface quality, eliminating shallow trap levels, and enhancing reliability properties. In summary, the effect of dual plasma treatment could be better than single plasma treatment and dual plasma treatment would be an effective technology to improve the reliability of $HfO_2$ thin films.

## Acknowledgments

The authors gratefully acknowledge the National Nano Device Laboratories (NDL) and the Nano Facility Center of the National Chiao Tung University.

## References

1. International Technology Roadmap for Semiconductors, presented at public.itrs.net (2009).
2. G. D. Wilk, R. M. Wallace, and J. M. Anthony, *J. Appl. Phys.*, **89**, 5243 (2001).
3. Y. Shimamoto, J. Yugami, M. Inoue, M. Mizutani, T. Hayashi, K. Shiga, F. Fujita, M. Yoneda, and H. Matsuoka, *Symposium on VLSI Technology Digest of Technical Papers*, IEEE, p. 132, (2005).
4. C. Hobbs, L. Fonseca, V. Dhandapani, S. Samavedam, B. Taylor, J. Grant, L. Dip, D. Triyoso, R. Hegde, D. Gilmer, R. Garcia, D. Roan, L. Lovejoy, R. Rai, L. Hebert, H. Tseng, B. White, and P. Tobin, *Symposium on VLSI Technology Digest of Technical Papers*, IEEE, p. 9, (2003).
5. J. Robertson, *J. Vac. Sci. Technol. B*, **18**, 1785 (2000).
6. S. Yamaguchi, K. Tai, T. Hirano, T. Ando, S. Hiyama, J. Wang, Y. Hagimoto, Y. Nagahama, T. Kato, K. Nagano, M. Yamanaka, S. Terauchi, S. Kanda, R. Yamamoto, Y. Tateshita, Y. Tagawa, H. Iwamoto, M. Saito, N. Nagashima, and S. Kadomura, *Symposium on VLSI Technology Digest of Technical Papers*, IEEE, p. 192, (2006).
7. J.-P. Han, E. M. Vogel, E. P. Gusev, C. D'Emic, C. A. Richter, D. W. Heh, and J. S. Suehle, *IEEE Electron Device Lett.*, **25**, 126 (2004).
8. G. Shang, P.W. Peacock, and J. Robertson, *Appl. Phys. Lett.*, **84**, 106 (2004).
9. K.M. Chang, B.N. Chen, and S.M. Huang, *Applied Surface Science,* **254**, 6116 (2008).
10. K.M. Chang, B.N. Chen, and C.K. Tang, *ECS Trans.*, **19** (2), 773 (2009).
11. C. H. Choi, S. J. Rhee, T. S. Jeon, N. Lu, J. H. Sim, R. Clark, M. Niwa, and D. L. Kwong, *Tech. Dig. - Int. Electron Devices Meet.*, **2002**, 857 (2002).
12. M. Koyama, A. Kaneko, T. Ino, M. Koike, Y. Kamata, R. Iijima, Y. Kamimuta, A. Takashima, M. Suzuki, C. Hongo, S. Inumiya, M. Takayanagi, and A. Nishiyama, *Tech. Dig. Int. Electron. Device Meet.*, p. 849, (2002).
13. N. Umezawa, K. Shiraishi, T. Ohno, H. Watanabe, T. Chikyow, K. Torii, K. Yamabe, K. Yamada, H. Kitajima, and T. Arikado, *Appl. Phys. Lett.*, **86**, 143507 (2005).
14. C.S. Lai, W.C. Wu, J.C. Wang, and T.S. Chao, *Appl. Phys. Lett.* **86**, 222905 (2005).
15. W.C. Wu, C.S. Lai, J.C. Wang, J.H. Chen, M.W. Ma, and T.S. Chao, *J. Electrochem. Soc.*, **154** H561 (2007).

16. K. Tse and J. Robertson, *Appl. Phys. Lett.* **89**, 142914 (2006).
17. H. Wong, B. Sen, V. Filip, and M. C. Poon, *Thin Solid Films*, **504**, 192 (2006).
18. K.I. Seo, R. Sreenivasan, P.C. McIntyre, and K.C. Saraswat, *Tech. Dig. - Int. Electron Devices Meet*, pp. 17.2.1–17.2.4., (2005).
19. C.S. Lai, W.C. Wu, K.M. Fan, J.C. Wang, and S.J. Lin, *Jpn. J. Appl. Phys.*, **44**, pp. 2307-2310, (2005)
20. C.S. Lai, W.C. Wu, T.S. Chao, J.H. Chen, J.C. Wang, L.L. Tay, and N. Rowell, *Appl. Phys. Lett.* **89**, 072904 (2006).
21. G. D. Wilk, M. L. Green, M.-Y. Hot, B. W. Busch, T. W. Sorsch, F. P. Klemens, B. Brijs', R. B. van Dover, A. Komblit, T. Gustafsson, E. Garfunkel, S. Hillenius, D. Monroe, P. Kalavade, and J.M. Hergenrother, *Symposium on VLSI Technology Digest of Technical Papers*, IEEE, p. 88, (2002).
22. J. Molina, K. Tachi, K. Kakushima, P. Ahmet, K. Tsutsui, N. Sugii, T. Hattori, and H. Iwai, *J. Electrochem. Soc.*, **154**, 110 (2007).
23. C.C. Cheng, C.H. Chien, C.W. Chen, S.L. Hsu, C.H. Yang, and C.Y. Changa, *J. Electrochem. Soc.*, **153**, 160 (2006).
24. M. R. Visokay, J. J. Chambers, A. L. P. Rotondaro, A. Shanware, and L. Colombo, *Appl. Phys. Lett.*, **80**, 3183 (2002).
25. H. X. Xu, J. P. Xu, C. X. Li, and P. T. Lai, *Appl. Phys. Lett.*, **97**, 022903 (2010).
26. T.M. Pan, C.S. Liao, H.H. Hsu, C.L. Chen, J.D. Lee, K.T. Wang, and J.C. Wang, *Appl. Phys. Lett.*, **87**, 262908 (2005).
27. H. Kim, C. O. Chui, K. C. Saraswat, and P. C. McIntyre, *Appl. Phys. Lett.*, **83**, 2647 (2003).
28. H. Harris, K. Choi, N. Mehta, A. Chandolu, N. Biswas, G. Kipshidze, and S. Nikishin, *Appl. Phys. Lett.*, **81**, 1065 (2002).
29. D. J. DiMaria, E. Cartier, and D. A. Buchanan, *J. Appl. Phys.*, **80**, 304 (1996).
30. M. Houssa, J. L. Autran, A. Stesmans, and M. M. Heyns, *Appl. Phys. Lett.*, **81**, 709 (2002).
31. E. Efthymiou**,** S. Bernardini**,** J.F. Zhang**,** S.N. Volkos**,** B. Hamilton**,** and A.R. Peaker**,** *Thin Solid Film*, **517**, 207 (2008).
32. W.C. Wu, C.S. Lai, T.M. Wang, J.C. Wang, C.W. Hsu, M.W. Ma, W.C. Lo, T.S. Chao, *IEEE Trans. Electron Devices*, 55, no. 7, pp. 1639–1646 (2008).
33. W.J. Zhu, T. P. Ma, T. Tamagawa, J. Kim, and Y. Di, *IEEE Electron Device Lett.*, **23**, 97 (2002).
34. F.C. Chiu, *J. Appl. Phys.*, **100**, 114102 (2006).
35. C.H. Liu, H.W. Chen, S.Y. Chen, H.S. Huang, and L.W. Cheng, *Appl. Phys. Lett.*, **95**, 012103 (2009).
36. F. El Kamel, P. Gonon, C. Vallée, and C. Jorel, J. Appl. Phys., **106**, 064508 (2009).
37. K.F. Schuegraf, and C. Hu, *J. Appl. Phys.*, **76**, 3695 (1994).